Diffusive over-hydration of olivine-hosted melt inclusions
Supplementary information and figures

ME Hartley, DA Neave, J Maclennan, M Edmonds, T Thordarson

Sample selection

The samples used in this study comprise fresh, glassy magmatic tephra from proximal fall deposits around the Laki cone row; quenched glassy selvages from the upper and/or lower surfaces of Laki lava flow surfaces (Hartley et al., 2014); and quenched, glassy pillow rims from Skuggafjöll mountain (Neave et al., 2014a). Olivine macrocrysts in the size range 250-1000 μm were picked from crushed samples of Laki lava and tephra samples. Olivine macrocrysts from Skuggafjöll were selected from the 500-1000 μm size fraction of crushed glassy samples. For all samples, care was taken to select pale green, unaltered olivines containing glassy melt inclusions without post-entrapment daughter crystals. Many of the olivine macrocrysts selected comprise partial crystal fragments rather than intact single crystals, since the macrocrysts often fractured during the crushing process. This was particularly the case for Skuggafjöll olivines.

Melt inclusion and olivine radii for diffusion modelling

Melt inclusion dimensions were measured from high resolution, high magnification photomicrographs using Zeiss AxioVision software, and were used to calculate the inclusion volume. For elliptical inclusions, we assumed that the inclusion depth was equal to the shorter of the measured dimensions. These volumes were then used to calculate a representative melt inclusion radius for use in diffusion models, which assume a spherical melt inclusion at the centre of a spherical olivine. The Laki melt inclusions discussed in this study were modelled using calculated radii ranging from 11.4 to 111 μm. Skuggafjöll melt inclusion radii ranged from 18.7 to 154 μm.

Radii of Laki olivines were estimated from photomicrographs of the inclusion-bearing crystals. In many cases the apparent crystal morphology has been modified by polishing and/or fracturing of the crystal during sample preparation. The apparent crystal size is also dependent on the cut through the crystal, and the extent of polishing required to expose the melt inclusion at the surface. The measured radii of the Laki olivines ranged from 225 to 550 μm. In the case of elongate or irregularly shaped crystals, the average of the longest and shortest axes is taken as a representative crystal radius.

Skuggafjöll olivines are generally equant, subhedral and range from 150 to 1500 μm in diameter. Rare olivines up to 4 mm in diameter are also present (Neave et al., 2014b). However, estimating the radii of the Skuggafjöll olivines used in this study is non-trivial since almost all the inclusion-bearing macrocrysts comprise crystal fragments generated during the crushing process. These fragments must originate from larger, unbroken macrocrysts. We therefore assume a radius of 750 μm for Skuggafjöll olivines, since macrocrysts of this size are common in Skuggafjöll samples. By assuming a large radius for the Skuggafjöll olivines, our calculated H^+ diffusion timescales are likely to represent maxima.

Analytical methods

Here we present a short overview of the analytical methods used to obtain the major, trace and volatile element data for the melt inclusions and olivines discussed in this study. For full details of all procedures, and to obtain copies of the datasets used in this study, please refer to Hartley et al. (2014) and Neave et al. (2014a).

Secondary ion mass spectrometry (SIMS)

All SIMS measurements were made using the Cameca ims-4f instrument at the NERC Ion Microprobe Facility at the University of Edinburgh, in four analytical sessions between May 2012 and April 2013. Measurements were made using a primary O^- beam with an accelerating voltage of 15 kV, a beam current of 5±1 nA, a secondary accelerating voltage of 4500 V minus an offset of -75±5 V, and a 25 μm image field. Analyses were made with a spot size of approximately 20 μm diameter.

Measurements on Laki melt inclusions and glass consisted of 10 cycles, including the following isotopes with counting times in parentheses: ^{1}H (4); ^{30}Si (2); ^{140}Ce (3). Measurements on Skuggafjöll melt inclusions and glass consisted of 6 cycles, including the following isotopes with counting times in parentheses: ^{1}H (5); ^{30}Si (2); ^{140}Ce (3). All peak positions were verified before each analysis. Mass 130.5 was measured to determine background levels in each cycle, and was always sufficiently close to zero to be ignored.

Silicate glass NIST-SRM610 was used as the calibration standard for trace elements. For each analytical session, ion yields from the first morning of analytical work were used to calibrate all of the melt inclusion data. Concentrations were calculated by normalising ^{30}Si to SiO_2, which was determined subsequently by electron microprobe at the University of Cambridge. International glass standards including ML3B-G, BCR2-G, GSD-1G and KL2-G, were used to monitor the calibration and instrumental drift, which was shown to be insignificant.

H_2O concentrations were calculated using a calibration curve constructed using a suite of basaltic glass standards containing between 0 and 3 wt.% H_2O (Shishkina et al., 2010), with ^{1}H counts normalised to ^{30}Si to account for the variations in the SiO_2 content of the standards. A new calibration curve was constructed each time minor changes were made to the analytical set-up.

SIMS data quality

The raw SIMS data was examined in order to exclude the possibility of contamination by the ion beam drilling through melt inclusions into the host mineral or an unnoticed phenocryst. Such contamination can be identified by monitoring the number of counts on a particular element over the number of cycles of the SIMS analysis (Fig. S1).

Basaltic glasses containing ~50 wt.% SiO_2 yield ^{30}Si count rates of the order 50,000-150,000 counts per cycle. Olivine contains ~38-40 wt.% SiO_2; thus, if the ion beam begins to sample olivine rather than pure glass, then a sharp and continuous decrease in ^{30}Si counts is observed over the remainder of the analysis. An example of a melt inclusion analysis contaminated by drilling into its host olivine is shown by the red dashed line in Fig. S1(a-c), and analyses of olivine made using the same analytical set-up as for the melt inclusions are shown by green dashed lines in Fig. S1(d-f). Analyses

contaminated by olivine can be readily idenfitied and rejected on the basis of sharp decreases in ^{30}Si counts and/or near-zero counts on incompatible trace elements such as Ce and Sr. None of the Laki or Skuggafjöll analyses used in this study show such trends.

Contamination by the ion beam sampling a host plagioclase crystal (∼45 wt.% SiO_2) has little discernible effect on ^{30}Si counts, but produces a marked and continuous increase in the Sr content of the analysis, since the partition coefficient for Sr in plagioclase is ≈2 (e.g. McKenzie and O'Nions, 1991). An example of a melt inclusion analysis contaminated by drilling into its plagioclase host is shown by the brown dashed line in Fig. S1(d-f).

While every effort was made to ensure that all melt inclusions analysed were glassy, we inspected the SIMS data for any indications that the ion beam sampled unnoticed post-entrapment daughter crystals of olivine, plagioclase or pyroxene. Accidental analysis of these mineral phases results in marked decreases in count rates for highly incompatible trace elements such as Ce, Y, Zr and Ba. None of our SIMS analyses show significant troughs in incompatible element counts which might indicate the presence of a daughter crystal. We are therefore confident that all SIMS analyses are free from mineral contaminants.

Electron probe microanalysis (EPMA)

Following SIMS analyses, major element compositions of glasses, melt inclusions and their host olivines were determined by Cameca SX100 instrument at the University of Cambridge, UK. Glass analyses were performed with a spot size of 10 Îijm, an operating potential of 15 kV and a beam current of 10 naA (Laki) or 6 nA (Skuggaföll). Olivine analyses were performed with an operating potential of 15 kV and a beam current of 20 nA (Laki) or 10 nA (Skuggafjöll). Concentrations of major and minor elements were determined in WDS mode with a peak count time of between 10 and 60 seconds depending on the abundance of the element within the mineral or glass under analysis. The instrument was calibrated at the start of every session using the following standards: Si glass or diopside for Si; diopside for Ca; rutile for Ti; corundum for Al; fayalite for Fe; olivine or periclase for Mg; jadeite for Na; K-feldspar for K; apatite for P; and pure metals for Mn, Cr and Ni. Data reduction was performed using inbuilt Cameca X-Phi PeakSight software for glass analyses and PAP corrections for mineral analyses. Most analyses returned totals of 98.5âĂŞ100.5 wt.%; analyses with totals outside this range or with inappropriate stoichiometry were discarded. 1σ precision estimates based on repeat measurements of standards are better than ±1% for SiO_2, TiO_2 and K_2O; better than ±2% for Al_2O_3, FeO, MgO and CaO; and better than ±5% for all other elements.

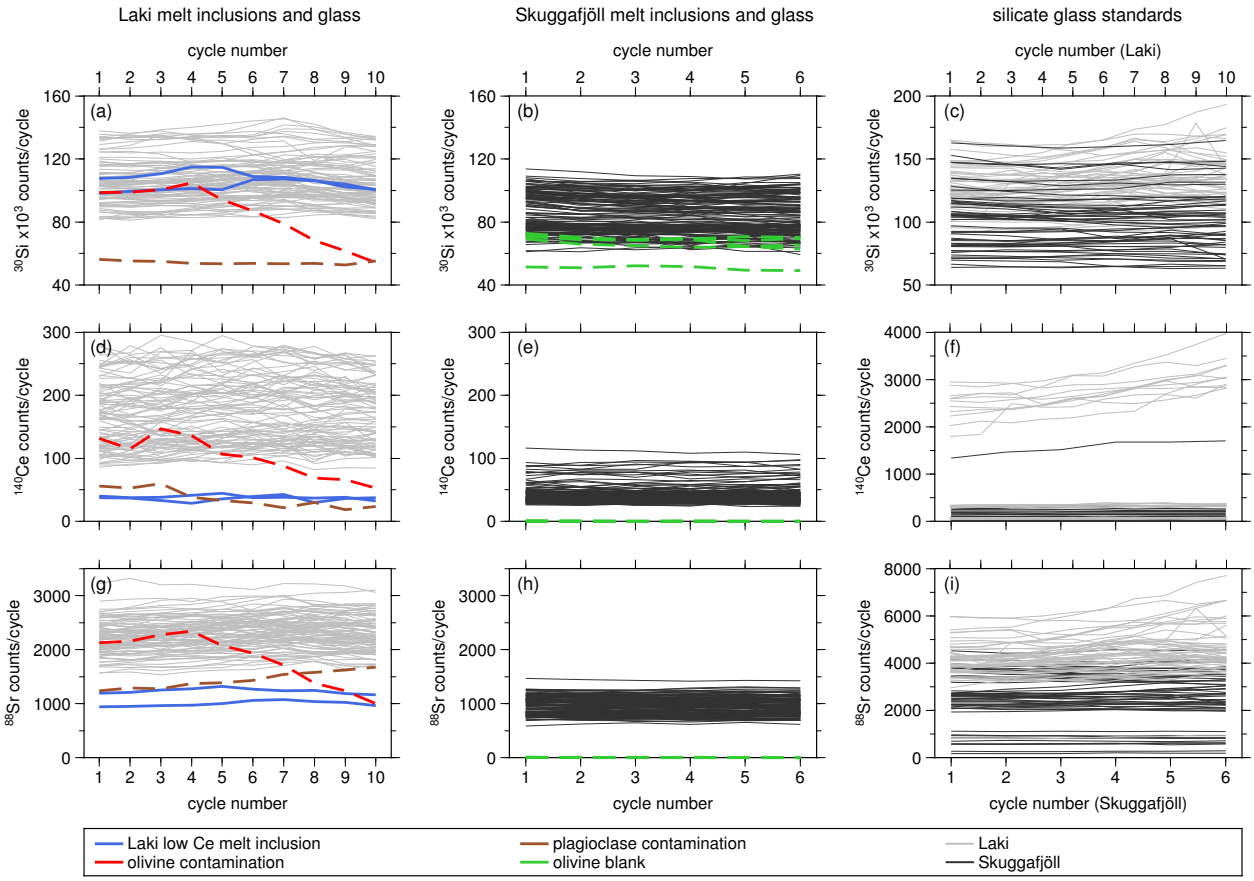

Figure S1. Counts per cycle of ^{30}Si, ^{140}Ce and ^{88}Sr for Laki and Skuggafjöll melt inclusions and glasses, and silicate glass standards, analysed by SIMS. The red dashed line shows an analysis of an olivine-hosted melt inclusion that has been contaminated by ion beam drilling through the inclusion into the host olivine, which is marked by a sharp decrease in measured counts on ^{30}Si and other incompatible trace elements. The brown dashed line shows an analysis of a plagioclase-hosted melt inclusion from Holuhraun, North Iceland, that has been contaminated by the ion beam drilling into the host plagioclase. Although there is little effect on ^{30}Si counts, there is a marked increase in measured ^{88}Sr counts. Green dashed lines show analyses of Skuggafjöll olivines made using the same analytical set-up as for the melt inclusions. The two blue lines represent olivine-hosted melt inclusions from Laki with very low measured Ce concentrations and high H_2O/Ce (Ce≈6 ppm; H_2O/Ce>800). These measurements show no evidence of contamination by the host olivine.

Position of melt inclusions within the host olivine

Experimental studies of the diffusive dehydration of olivine-hosted melt inclusions document positive correlations between melt inclusion H_2O content and host olivine size (e.g. Chen et al., 2011; Bucholz et al., 2013). Conversely, diffusive re-equilibration between melt inclusions and a more hydrous carrier melt is expected to generate a negative correlation between melt inclusion H_2O content and host olivine size. For melt inclusions in Laki tephra samples, we find a very weak negative correlation (r^2=0.25) between melt inclusion H_2O content and olivine radius (Fig. S2) which is consistent with diffusive over-hydration of these inclusions. No correlation exists between melt inclusion H_2O and olivine radius for dehydrated melt inclusions in Laki lava samples, indicating near-complete re-equilibration between the inclusions and the degassed Laki lava during insulated transport. Skuggafjöll olivines used in this study are primarily crystal fragments originating from macrocrysts of unknown size, so it was not possible to investigate the relationship between melt inclusion H_2O and host olivine size. However, Skuggafjöll melt inclusions have very uniform H_2O contents of 0.38±0.05 wt.% (2σ), indicating that most inclusions were close to equilibrium with their carrier melt.

Compositional differences between melt inclusions located at different distances from the surfaces of their host olivines may reflect the evolution of the magma from which the inclusions were trapped. A negative correlation between melt inclusion H_2O and distance from the host olivine surface is therefore expected for inclusions trapped from an evolving magma. However, for a suite of natural olivine-hosted melt inclusions from Cerro Negro volcano, Nicaragua, Bucholz et al. (2013) noted a positive correlation between melt inclusion H_2O content and the distance between the inclusion and the host olivine surface, a trend that is indicative of diffusive dehydration in the inclusions nearest the olivine surface. Negative correlations between melt inclusion H_2 content and distance from olivine surface may be generated by the trapping of an evolving magma and/or by diffusive over-hydration of inclusions nearest the olivine surface. Concentrations of slowly diffusing incompatible trace elements are therefore required to distinguish between these two processes. For the EVZ melt inclusions in this study, we found no correlation between melt inclusion composition and the shortest distance between the inclusion and the edge of its host olivine.

Backscattered electron images of Laki and Skuggafjöll olivines and QEMSCAN images of Skuggafjoll thin sections (Neave et al., 2014b) indicate that typical EVZ olivines have uniform core compositions surrounded by thin overgrowth rims of a less forsteritic composition. For Laki olivines, these low-forsterite rims are typically no more than ∼40-60 μm in width and rarely exceed 100 μm. For Skuggafjöll olivines, the rims are typically ∼80-100 μm, with a maximum width of ∼150-180 μm (Neave et al., 2014b). All of the EVZ melt inclusions in this study were surrounded by olivine of uniform composition, and none of the inclusions extended into the low-forsterite rims of their host olivines. We therefore consider all of the inclusions to be located in the cores of their host olivines, and that olivine core compositions provide the best proxy for the degree of melt evolution at the time of inclusion trapping.

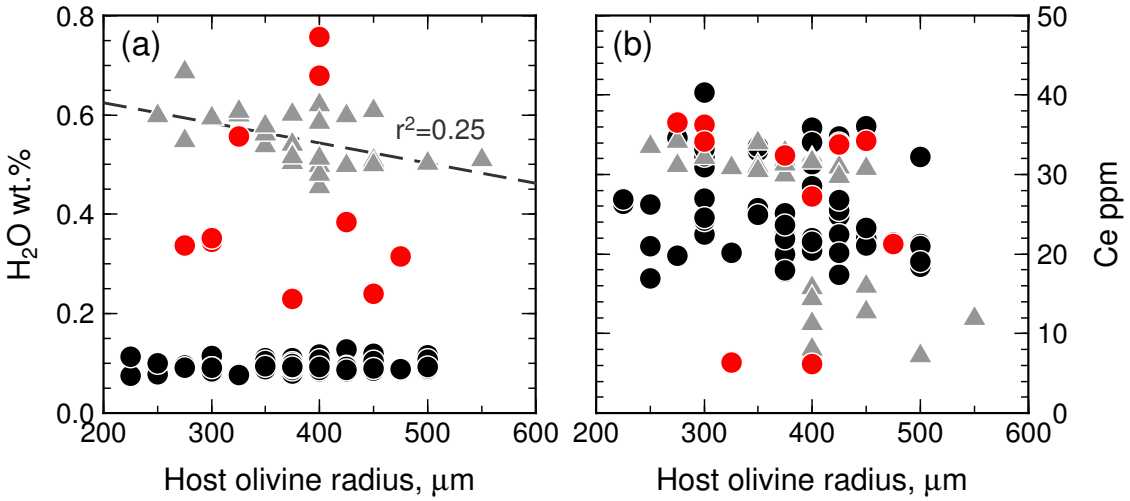

Figure S2. Relationship between Laki melt inclusion compositions and host olivine radius. Triangles show melt inclusions from Laki lava samples; circles show melt inclusions from Laki lava samples. The red circles show melt inclusions from lava samples that have not completely re-equilibrated with the degassed Laki carrier melt. (a) Melt inclusions from Laki tephra samples show a weak correlation between melt inclusion H_2) and host olivine radius. There is no correlation for inclusions from lava samples. (b) There is no relationship between melt inclusion Ce content and host olivine radius.

Partition coefficients for reverse fractional crystallisation modelling

	Ce		Y	
$D^{ol-melt}$	0.0001	*a*	0.005	*d*
$D^{cpx-melt}$	0.108	*b*	0.6	*e*
$D^{plg-melt}$	0.05	*c*	0.085	*c*

Table S1. Partition coefficients used in the reverse fractional crystallisation models described in Section 4.1 of the main text. References: *a*, Spandler et al. (2007); *b*, Hauri et al. (1994); *c*, Aigner-Torres et al. (2007); *d*, Beattie (1994); *e*, Hack et al. (1994). The Spandler et al. (2007) value for $D^{ol-melt}_{Ce}$ was determined using the same experimental conditions and olivine compositions as the diffusion coefficient for Ce in olivine that we use for diffusion modelling in Section 5.5 of the main text.

Relationship between melt inclusion composition and host olivine composition

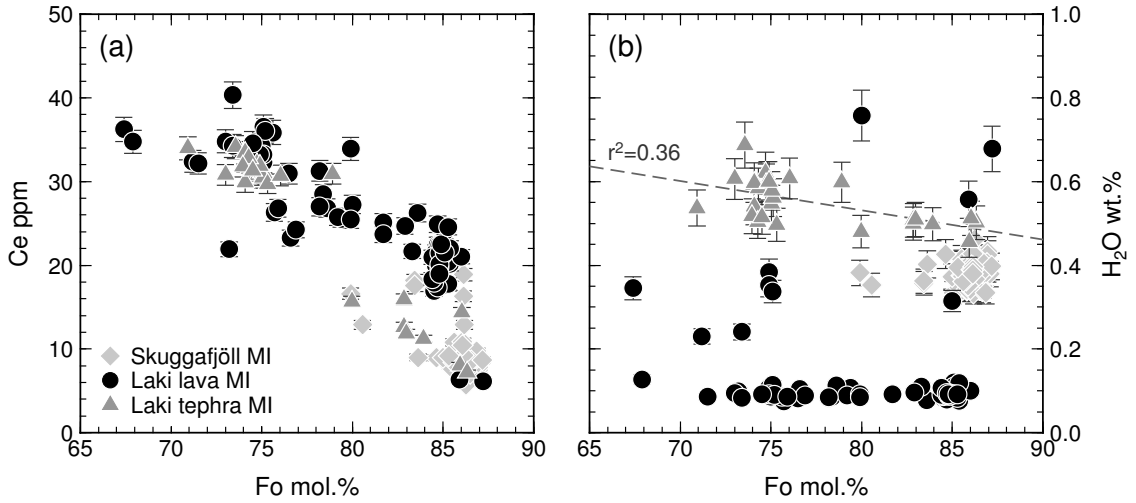

Figure S3. (a) EVZ melt inclusions show a strong correlation between their Ce contents and host olivine forsterite, indicating that the melt inclusion Ce contents are largely controlled by fractional crystallisation. (b) There is no relationship between melt inclusion H_2O and host olivine composition, indicating that fractional crystallisation is not the primary control on melt inclusion H_2O contents. The weak negative correlation between H_2O and Fo for Laki tephra melt inclusions is not significant when analytical uncertainties are taken into account.

H_2O and the formation of bubbles in melt inclusions

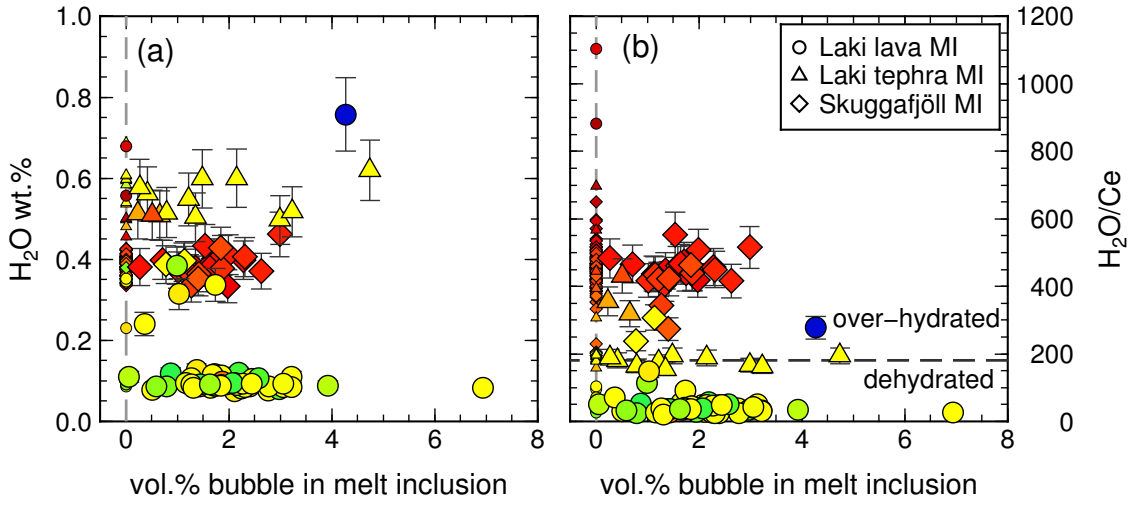

Figure S4. (a) Melt inclusion H_2O and (b) H_2O/Ce vs. the volume of the melt inclusion occupied by a bubble for Laki and Skuggafjöll inclusions.

Several of the EVZ melt inclusions contain bubbles, which formed in response to cooling and thermal contraction of the glass phase upon eruption. Bubbles in melt inclusions from Laki lava samples contain CO_2 vapour, which diffused into the bubble during post-eruptive insulated transport within lava flows (Hartley et al., 2014). Melt inclusions hosted in olivines from Skuggafjöll and Laki tephra samples were quenched rapidly upon eruption, and bubbles in these inclusions are CO_2-free (Neave et al., 2014a).

Volatile concentrations in melt inclusions are sensitive to post-entrapment crystallisation (PEC) on the inclusion walls, which causes volatile element enrichment in the melt phase. PEC promotes the exsolution of CO_2 into a vapour phase, with a resultant drop in the CO_2 content of the melt (Steele-MacInnis et al., 2011). The H_2O content of the melt phase increases as PEC continues, due to the slight increase in H_2O solubility with decreasing temperature (Blundy and Cashman, 2008; Steele-MacInnis et al., 2011). H_2O is not expected to degas into the bubble.

The EVZ melt inclusions underwent a maximum of 7% PEC, with most inclusions undergoing <2% PEC (Hartley et al., 2014; Neave et al., 2014a). For PEC<5% the increase in melt H_2O content is expected to be ~5-10%, which is smaller than the analytical uncertainty of the H_2O measurements. There is no correlation between PEC and melt H_2O content. None of the EVZ inclusion-hosted bubbles contain H_2O vapour (Hartley et al., 2014; Neave et al., 2014a), and there is no correlation between the volume of the melt inclusion occupied by a bubble and melt H_2O content; nor between bubble vol.% and melt H_2O/Ce (Fig. S4). These observations indicate that H_2O contents in the EVZ melt inclusions have not been significantly modified by PEC.

Trapping of enriched boundary layers

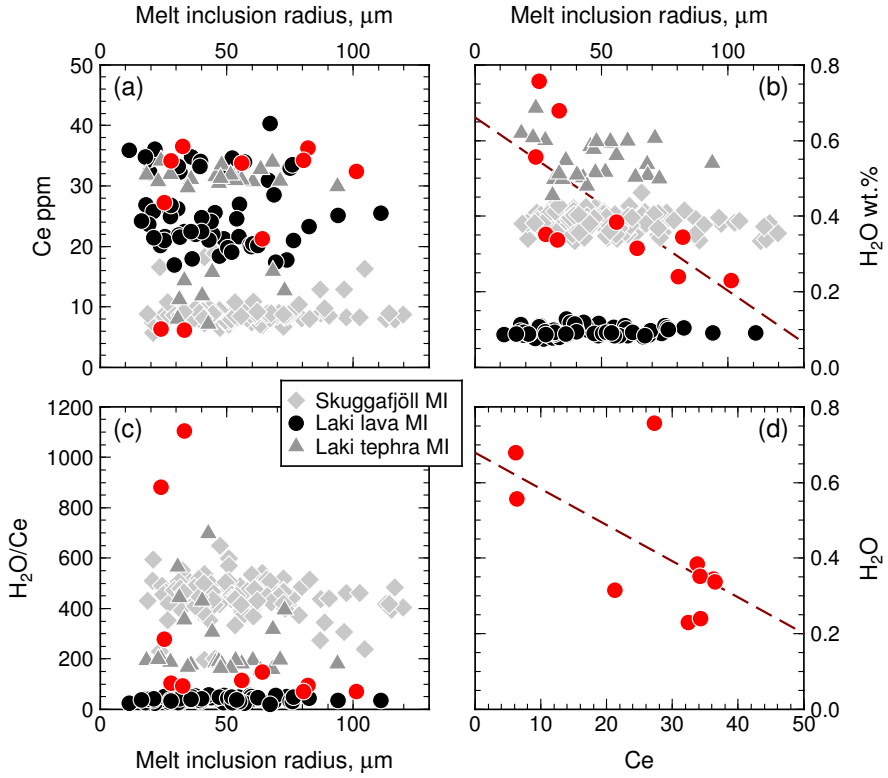

Figure S5. Melt inclusion composition vs. melt inclusion radius. The red symbols show a subset of melt inclusions from Laki lava samples for which H_2O content is negatively correlated with melt inclusion radius.

Melt inclusions that trapped an incompatible element enriched boundary layer are expected to show negative correlations between incompatible element abundances and melt inclusion size. This is explored in Fig. S5. We find no correlation between melt inclusion Ce content and inclusion size, nor between melt inclusion H_2O/Ce and inclusion size. Most of the EVZ inclusions show no relationship between inclusion radius and H_2O; however, a subset of 10 melt inclusions from Laki lava samples form a negative correlation (r^2=0.50) between H_2O and inclusion radius (Fig. S5b). This subset includes the two most depleted Laki melt inclusions. If this correlation between inclusion size and H_2O were due to the trapping of an enriched boundary layer, a corresponding positive correlation between Ce and H_2O might be expected. However, Ce and H_2O contents are negatively correlated (r^2=0.40) in these inclusions (Fig. S5d).

Ce diffusion in basaltic melt is very slow compared to H_2O diffusion (Zhang et al., 2010) which suggests that a negative correlation between Ce and inclusion size is a better diagnostic test of boundary layer trapping than any correlation between inclusion size and H_2O. The lack of correlation between melt inclusion size and Ce suggests that boundary layer trapping is not a feature of the EVZ dataset. The correlation shown by the Laki lava inclusions highlighted in Fig. S5b is most probably related to diffusional processes.

Determination of H_2O/Ce for Icelandic primary melts

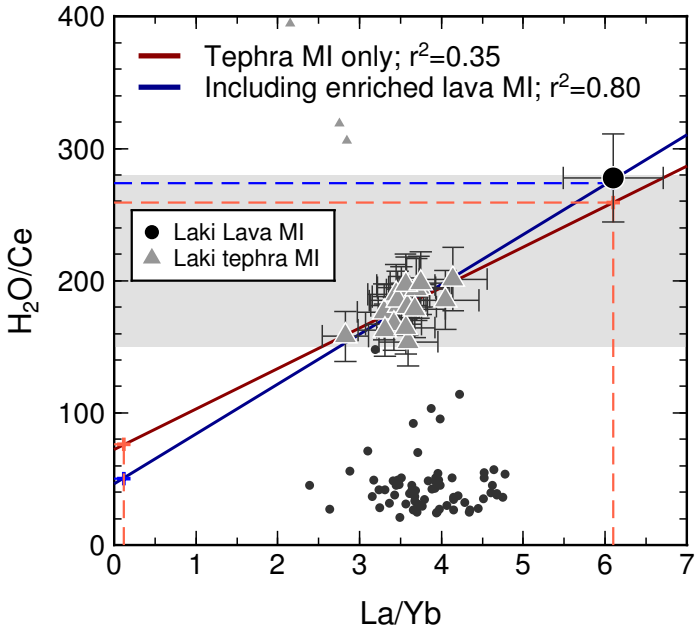

Figure S6. The relative incompatibility of H_2O and Ce varies systematically for depleted MORB samples with La/Sm<1.5 (Danyushevsky et al., 2000; Dixon and Clague, 2001). Undegassed, enriched primary melts with high initial Ce concentrations might therefore be expected to have high H_2O concentrations and higher H_2O/Ce than depleted primary melts.

Potential H_2O/Ce values for enriched and depleted EVZ endmember melts were investigated using the above plot of H_2O/Ce vs. La/Yb for Laki melt inclusions with measured H_2O/Ce within the expected range for MORB glasses of $150<H_2O/Ce<280$, shown by the grey shaded box. The blue dashed line shows the best-fit linear regression including the enriched inclusion. The strength of this correlation is largely defined by a single highly enriched inclusion with H_2O/Ce significantly higher than for melt inclusions from tephra samples. The red dashed line shows the best-fit linear regression for inclusions from tephra samples only; the correlation is much weaker. The correlations between La/Yb and H_2O/Ce can be used to estimate H_2O/Ce values for the most enriched and depleted primary melts generated under Iceland. Thin dashed lines show La/Yb for the most enriched and most depleted melt inclusion compositions found in Iceland (Maclennan, 2008), and their corresponding H_2O/Ce values according to the correlations shown. The small symbols show melt inclusions with H_2O/Ce outwith the expected MORB range.

The poor correlation between H_2O/Ce and La/Yb for Laki tephra melt inclusions means that there is considerable uncertainty in the H_2O/Ce values for enriched and depleted endmembers obtained from the regressions. In particular, the calculated H_2O/Ce for the depleted endmember lies far outwith the expected range for MORB glasses and is also much lower than the value of 168 obtained from highly depleted melt inclusions from the Siqueiros transform fault (Saal et al., 2002).

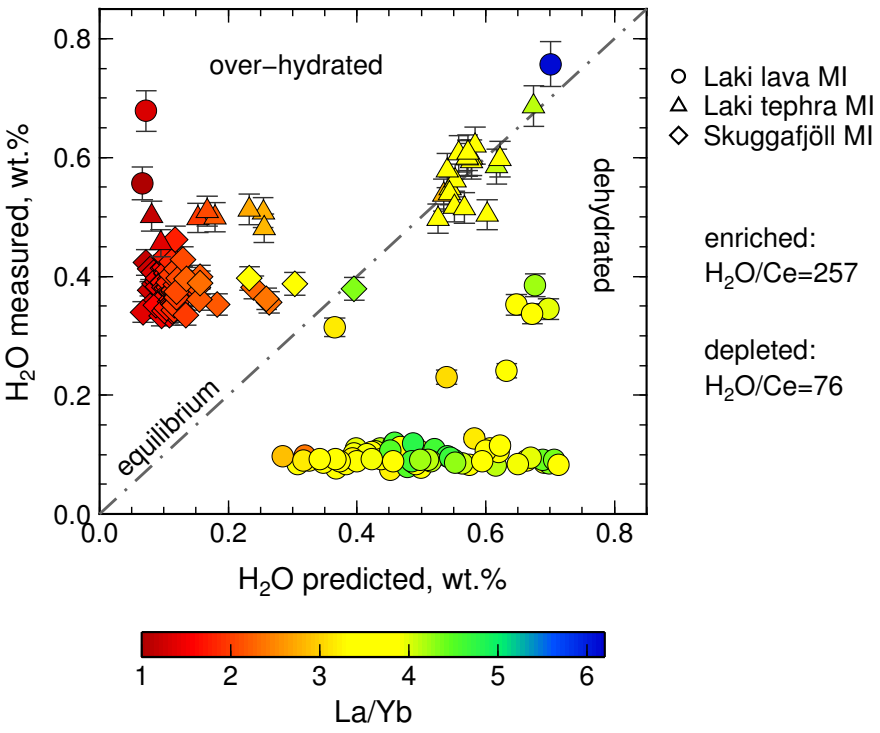

Figure S7. Predicted H_2O content of EVZ melt inclusions, calculated using the measured Ce content as a proxy for initial H_2O, vs. measured H_2O content, and coloured by La/Yb. H_2O/Ce is assumed to vary with primary melt composition according to the correlations shown in Fig. D; the H_2O/Ce values assumed for enriched and depleted endmembers are 257 and 76 respectively. The proportions of enriched and depleted primary melt endmembers and the extent of crystallisation required to generate the compositions of the EVZ melt inclusions were calculated according to the method of Maclennan (2008); these values were then used to calculate the expected initial H_2O/Ce for each inclusion. The three-fold distribution of 'equilibrium', dehydrated and over-hydrated melt inclusions is identical to that observed when H_2O/Ce in primary melts is assumed to be constant (Fig. 6 in the main text). The principal difference between the two methods is that the most enriched melt inclusion, with La/Yb=6.1, appears to be hydrated if constant initial H_2O/Ce is assumed, but appears to have be little affected by H^+ diffusion if variable initial H_2O/Ce is assumed.

References

Aigner-Torres, M., J. Blundy, P. Ulmer, and T. Pettke, 2007: Laser ablation ICPMS study of trace element partitioning between plagioclase and basaltic melts: an experimental approach. *Contributions to Mineralogy and Petrology*, **153**, 647–667.

Beattie, P., 1994: Systematics and energetics of trace-element partitioning between olivine and silicate melts: implications for the nature of mineral/melt partitioning. *Chemical Geology*, **117**, 57–71.

Blundy, J. and K. Cashman, 2008: Petrologic reconstruction of magmatic system variables and processes. *Reviews in Mineralogy and Geochemistry*, **69**, 179–239.

Bucholz, C. E., G. A. Gaetani, M. D. Behn, and N. Shimizu, 2013: Post-entrapment modification of volatiles and oxygen fugacity in olivine-hosted melt inclusions. *Earth and Planetary Science Letters*, **374**, 145–155.

Chen, Y., A. Provost, P. Schiano, and N. Cluzel, 2011: The rate of water loss from olivine-hosted melt inclusions. *Contributions to Mineralogy and Petrology*, **162**, 625–636.

Danyushevsky, L. V., T. J. Eggins, S. M.and Falloon, and D. M. Christie, 2000: H_2O abundance in depleted to moderately enriched mid-ocean ridge magmas; Part I: incompatible behaviour, implications for mantle storage, and origin of regional variations. *Journal of Petrology*, **41**, 1329–1364.

Dixon, J. E. and D. A. Clague, 2001: Volatiles in basaltic glasses from Loihi Seamount, Hawaii: Evidence for a relatively dry plume component. *Journal of Petrology*, **42**, 627–654.

Hack, P. J., R. L. Nielsen, and A. D. Johnston, 1994: Experimentally determined rare-earth element and Y partitioning behavior between clinopyroxene and basaltic liquids at pressures up to 20 kbar. *Chemical Geology*, **117**, 89–105.

Hartley, M. E., J. Maclennan, M. Edmonds, and T. Thordarson, 2014: Reconstructing the deep CO_2 degassing behaviour of large basaltic fissure eruptions. *Earth and Planetary Science Letters*, **393**, 120–131.

Hauri, E. H., T. P. Wagner, and T. L. Grove, 1994: Experimental and natural partitioning of Th, U, Pb and other trace elements between garnet, clinopyroxene and basaltic melts. *Chemical Geology*, **117**, 149–166.

Maclennan, J., 2008: Concurrent mixing and cooling of melts under Iceland. *Journal of Petrology*, **49**, 1931–1953.

McKenzie, D. and R. K. O'Nions, 1991: Partial melt distributions from inversion of rare-earth element concentrations. *Journal of Petrology*, **32**, 1021–1091.

Neave, D. A., J. Maclennan, M. Edmonds, and T. Thordarson, 2014a: Melt mixing causes negative correlation of trace element enrichment and CO_2 content prior to an Icelandic eruption. *Earth and Planetary Science Letters*, **400**, 272–283.

Neave, D. A., J. Maclennan, M. E. Hartley, M. Edmonds, and T. Thordarson, 2014b: Crystal storage and transfer in basaltic systems: the Skuggafjöll eruption, Iceland. *Journal of Petrology*, **55**, 2311–2346.

Saal, A. E., E. H. Hauri, C. H. Langmuir, and M. R. Perfit, 2002: Vapour undersaturation in primitive mid-ocean-ridge basalt and the volatile content of Earth's upper mantle. *Nature*, **419**, 451–455.

Shishkina, T. A., R. E. Botcharnikov, F. Holtz, R. R. Almeev, and M. V. Portnyagin, 2010: Solubility of H_2O-and CO_2-bearing fluids in tholeiitic basalts at pressures up to 500 MPa. *Chemical Geology*, **277**, 115–125.

Spandler, C., H. S. C. O'Neill, and V. S. Kamenetsky, 2007: Survival times of anomalous melt inclusions from element diffusion in olivine and chromite. *Nature*, **447**, 303–306.

Steele-MacInnis, M., R. Esposito, and R. J. Bodnar, 2011: Thermodynamic model for the effect of post-entrapment crystallization on the H_2O-CO_2 systematics of vapor-saturated, silicate melt inclusions. *Journal of Petrology*, **52**, 2461–2482.

Zhang, Y., H. Ni, and Y. Chen, 2010: Diffusion data in silicate melts. *Reviews in Mineralogy and Geochemistry*, **72**, 311–408.